

Solvent Quality Dependent Osmotic Pressure of Polymer Solutions in Two Dimensions

Published as part of *The Journal of Physical Chemistry virtual special issue "Jose Onuchic Festschrift"*.

Lei Liu* and Changbong Hyeon*



Cite This: *J. Phys. Chem. B* 2022, 126, 9695–9704



Read Online

ACCESS |



Metrics & More

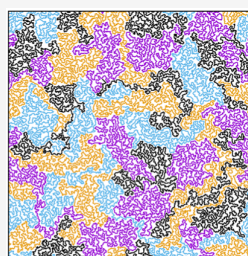


Article Recommendations



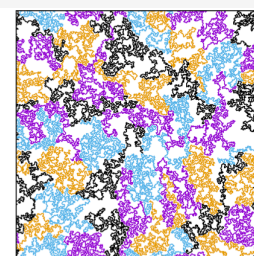
Supporting Information

ABSTRACT: Confined in two-dimensional planes, polymer chains comprising dense monolayer solutions are segregated from each other because of topological interaction. Although the segregation is inherent in two dimensions (2D), the solution may display different properties depending on the solvent quality. Among others, it is well-known in both theory and experiment that the osmotic pressure (Π) in the semidilute regime displays solvent quality dependent increases with the area fraction (ϕ) (or monomer concentration, ρ), that is, $\Pi \sim \phi^3$ for good solvents and $\Pi \sim \phi^8$ for Θ solvents. The osmotic pressure can be associated with the Flory exponent (or the correlation length exponent) for the chain size and the pair distribution function of monomers; however, they do not necessarily offer a detailed microscopic picture leading to the difference. To gain microscopic understanding into the different surface pressure isotherms of polymer solutions under the two distinct solvent conditions, we study the chain configurations of the polymer solution based on our numerical simulations that semiquantitatively reproduce the expected scaling behaviors. Notably, at the same value of ϕ , polymer chains in a Θ solvent occupy the surface in a more *inhomogeneous* manner than the chains in good solvent, yielding on average a greater and more heterogeneous interstitial void size, which is related to the fact that the polymer in the Θ solvent has a greater correlation length. The polymer configurations and interstitial voids visualized and quantitatively analyzed in this study offer microscopic understanding to the origin of the solvent quality dependent osmotic pressure of 2D polymer solutions.



good solvent

VS



Θ solvent

INTRODUCTION

A flexible polymer chain in three dimensions (3D) exhibits a coil-to-globule transition with varying temperature (T) or solvent quality. The polymer size, the so-called Flory radius R_F , scales with the number of monomers (N) as $R_F \sim N^\nu$. The scaling exponent ν , known as the Flory exponent, which is tantamount to the correlation length exponent in the general context of critical phenomena,¹ changes from $\nu = 0.588$ (good, $T > \Theta$) to $\nu = 1/3$ (poor, $T < \Theta$) as the temperature is lowered. At $T \approx \Theta$, the exponent $\nu_{\Theta}^{3D} = 1/2$ is identical to that of the random walk (RW). The polymer chains in a Θ solvent are at a point where the attraction and repulsion between monomers compensate. The Θ point of a 3D polymer is determined as that at which the second virial coefficient vanishes ($B_2 = 0$). The higher-order virial terms contribute only logarithmically to the free energy so that the condition of $N \gg 1$ yields $R_F \sim N^{1/2}$.² In light of the polymer-magnet analogy, the condition $B_2 = 0$ amounts to the tricritical point of the Landau free energy.³

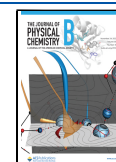
In two dimensions (2D), the correlation length exponent is $\nu_{\Theta}^{2D} = 4/7$, which is different from that of the RW. Since the higher-order virial terms cannot be ignored in 2D, the Θ point of a polymer chain in 2D is defined under a more subtle condition

than $B_2 = 0$ in 3D.^{4–6} As a result, the Θ point of a 2D polymer, in practice, has numerically been attained by tuning the relevant parameters⁷ (see the **Methods** section). Historically, studies on geometrical fractal objects in 2D, in particular, the Θ chain in 2D and its exotic exponent $\nu_{\Theta}^{2D} = 4/7 \approx 0.571$, culminated in the 1980s. Coniglio et al.⁷ posited that the fractal dimension ($\mathcal{D} = (\nu_{\Theta}^{2D})^{-1} = 7/4$) of the 2D *interacting* self-avoiding walk at the coil-to-globule transition point is identical to the dimension of percolating clusters' boundaries (hulls).^{8,9} Duplantier and Saleur showed, using the conformal invariance, that the 2D Θ chain, the hull of percolating clusters, and uncorrelated diffusion fronts in 2D at the scaling limit are all characterized with the fractal (Hausdorff) dimension of $7/4$ and belong to the same universality class.^{10–13} Later, this result was more rigorously proven as the Hausdorff dimension of the curve

Received: August 1, 2022

Revised: October 24, 2022

Published: November 9, 2022



($\mathcal{D} = \min(2, 1 + \kappa/8)$) generated from the stochastic Loewner evolution (SLE) process with parameter $\kappa = 6$, denoted by SLE_6 .¹⁴

The correlation length exponent ν of a 2D polymer has indirectly been determined through surface pressure (Π) measurements of thin polymer films formed at the air–water interface as a function of the area fraction of the polymer solution (ϕ).^{15,16} In the semidilute phase $\phi^* < \phi \ll 1$, where ϕ^* is the critical overlap area fraction (see Appendix A for the basics of osmotic pressure of polymer solutions with increasing ϕ), Π scales with ϕ as $\Pi \sim \phi^q$. Actual measurements of the surface pressure (or osmotic pressure) have shown that $q = 3$ for 2D polymer solutions in good solvents, whereas $q = 8$ in Θ solvents.^{15–17} Since the exponent q is related with ν as $q = 2\nu/(2\nu - 1)$ ¹ (see Appendix A), it can be deduced from $\Pi \sim \phi^q$ that a single polymer chain in 2D obeys $R_F \sim N^\nu$ with $\nu = 3/4 = 0.75$ and $\nu = 4/7 \approx 0.571$ under good and Θ solvent conditions, respectively. The difference between the exponents (q) of the osmotic pressure against ϕ in the semidilute phase under the two solvent conditions is significant. However, besides the difference in ν , it remains elusive how the ϕ -dependent configurations of individual polymer chains and their interface with neighboring chains contribute to the surface pressure under the two different solvent conditions.

Despite a number of extensive theoretical studies on the thermodynamics and conformational properties of 2D polymer solutions, their focus was predominantly on the solution made of self-avoiding polymers.^{18–24} Here, using theoretical arguments along with numerics, we aim to explore the microscopic underpinning that leads to the solvent quality dependent Π – ϕ isotherm of 2D polymer solutions. In this paper, we first demonstrate the main result of the Π – ϕ isotherm calculated from the simulations of polymer solutions composed of self-avoiding walks (SAWs) and Θ chains. We next discuss the difference of two polymer solutions in terms of the radial distribution of monomers ($g(r)$), solvent quality dependent conformations of individual polymer chains, and interstitial voids formed in polymer solutions. Our study highlights the distinct chain statistics and organization of a polymer solution under good and Θ solvent conditions, offering a clear picture of how these differences lead to distinct Π – ϕ isotherms of polymer solutions in 2D.

METHODS

Generating Θ Chains in Two Dimensions. The following energy potential was used to simulate a polymer chain composed of N segments:

$$\mathcal{H}(\mathbf{r}) = \mathcal{H}_b(\mathbf{r}) + \mathcal{H}_{nb}(\mathbf{r}) \quad (1)$$

where $\mathbf{r} = \{\mathbf{r}_i\}$ and \mathbf{r}_i denotes the coordinate of the i th monomer in a 2D plane. The first term models the chain connectivity with the finite extensible nonlinear elastic (FENE) potential and a shifted Weeks–Chandler–Anderson (WCA) potential:

$$\begin{aligned} \beta\mathcal{H}_b(\mathbf{r}) = & -\frac{\beta k}{2} R_c^2 \sum_{i=0}^{N-1} \log \left(1 - \frac{r_{i,i+1}^2}{R_c^2} \right) \\ & + \sum_{i=1}^N 4 \left[\left(\frac{a}{r_{i,i+1}} \right)^{12} - \left(\frac{a}{r_{i,i+1}} \right)^6 + \frac{1}{4} \right] H(2^{1/6}a - r_{i,i+1}) \end{aligned} \quad (2)$$

where $r_{i,i+1} \equiv |\mathbf{r}_{i+1} - \mathbf{r}_i|$ is the segment length, $H(\dots)$ is the Heaviside step function, and we chose the parameters $k = 30 k_B T$

with $R_c = 1.5a$. The energy potential with these parameters equilibrates the segments at $b_i \approx a$. The second term in eq 1 involves the nonbonded interactions between two different monomers. For a good solvent $\mathcal{H}_{nb}(\mathbf{r}) = \mathcal{H}_{nb}^{\text{good}}(\mathbf{r})$

$$\beta\mathcal{H}_{nb}^{\text{good}}(\mathbf{r}) = \sum_{i < j} 4 \left[\left(\frac{a}{r_{ij}} \right)^{12} - \left(\frac{a}{r_{ij}} \right)^6 + \frac{1}{4} \right] H(2^{1/6}a - r_{ij}) \quad (3)$$

and for a Θ condition $\mathcal{H}_{nb}(\mathbf{r}) = \mathcal{H}_{nb}^{\Theta}(\mathbf{r})$

$$\beta\mathcal{H}_{nb}^{\Theta}(\mathbf{r}) = \sum_{i < j} \varepsilon \left[\left(\frac{a}{r_{ij}} \right)^{12} - 2 \left(\frac{a}{r_{ij}} \right)^6 + \Delta_s \right] H(2.5a - r_{ij}) \quad (4)$$

where $r_{ij} = |\mathbf{r}_i - \mathbf{r}_j|$. For the Θ solvent, the Lennard-Jones potential was shifted upward by $\Delta_s = 2 \times 0.4^6 - 0.4^{12}$ such that the potential is continuous at $r_{ij} = 2.5a$, and the parameter ε was set to $\varepsilon_{\Theta} = 1.013$ which yields the scaling $R_{ee} \sim N^{4/7}$ (see Figure 1).

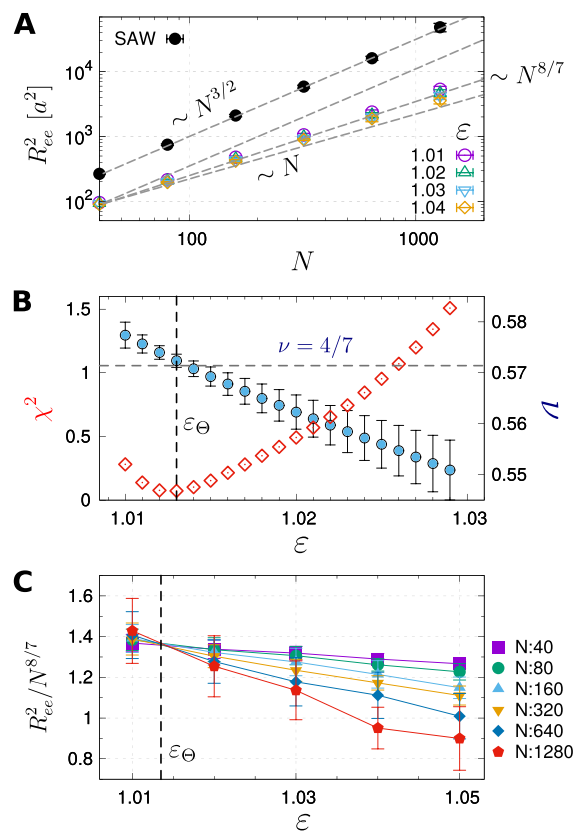


Figure 1. Single chain size scaling and the Θ condition in 2D. (A) While the end-to-end distance R_{ee} of the SAW chain shows the expected scaling behavior ($R_{ee}^2 \sim N^{3/2}$), the monomer attraction strength (ε) was fine-tuned such that $R_{ee}(N, \varepsilon)$ satisfies a power law $R_{ee}^2 \sim N^{2\nu}$ with some value of ν . (B) χ^2 and the best value of ν obtained by fitting the data at different values of ε to the power law. The most confident scaling relation with $\nu \simeq 4/7$ is acquired when $\varepsilon_{\Theta} \simeq 1.013$. (C) Alternatively, if we take Duplantier’s proposal $\nu = 4/7$ as granted, $R_{ee}^2/N^{2\nu}$ should become independent of N at the Θ condition, which again locates ε_{Θ} around 1.013 in our model.

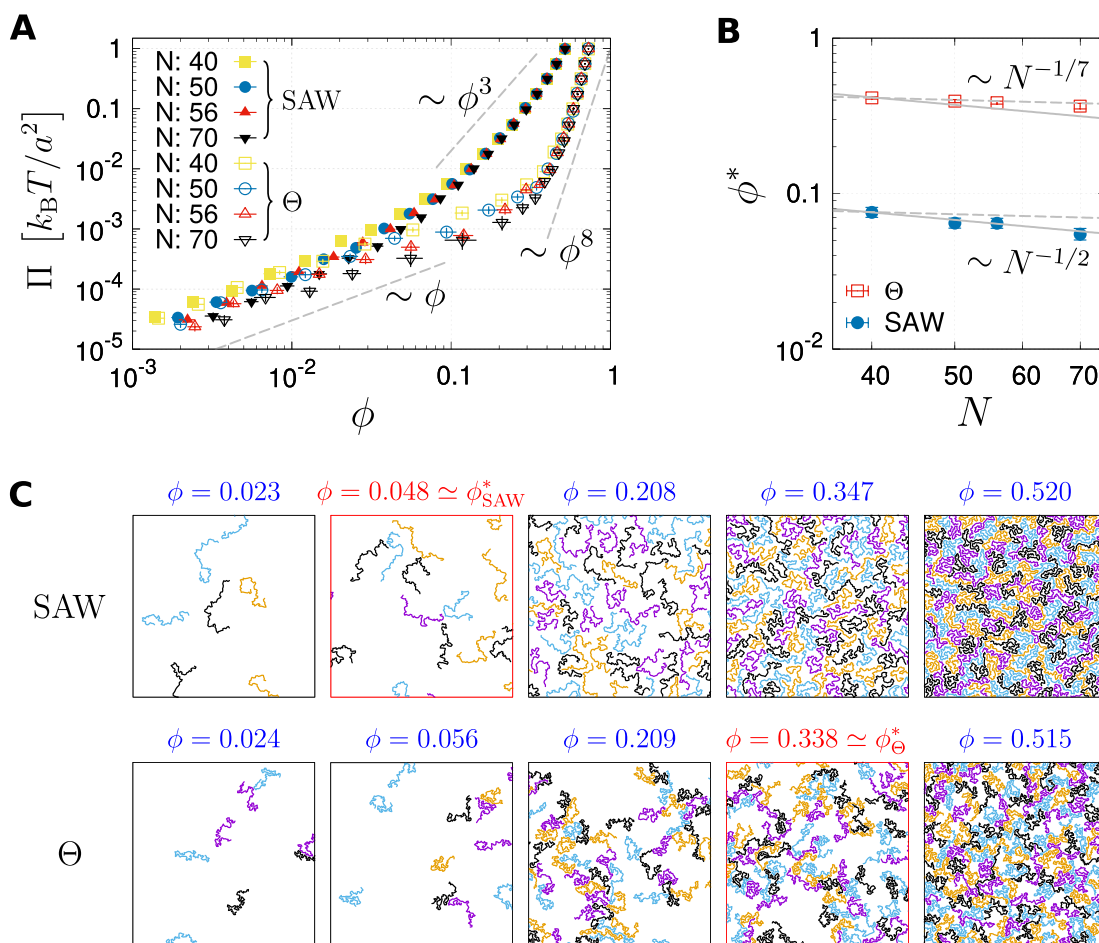


Figure 2. Difference between 2D polymer solutions made of SAW and Θ chains. (A) Π vs ϕ with varying N . (B) N -Dependent overlap fraction (ϕ^*) from dilute to semidilute solution. ϕ^* for each N is determined from the crossover point where the fits using ϕ and ϕ^3 (or ϕ and ϕ^8) lines meet in panel A. For $N = 70$, $\phi_{\text{SAW}}^* = 0.054 \pm 0.004$ and $\phi_{\Theta}^* = 0.365 \pm 0.015$. Dashed and solid lines are the N -dependencies expected for $\phi_{\Theta}^* \sim N^{-1/7}$ and $\phi_{\text{SAW}}^* \sim N^{-1/2}$. (C) From left to right, shown are the SAW (top row) and Θ polymer solutions (bottom row) with increasing ϕ , encompassing the nonoverlapping ($\phi/\phi^* < 1$), semidilute ($\phi/\phi^* \approx 1$), and dense melt regimes ($\phi/\phi^* \gg 1$). The panels corresponding to the area fraction close to ϕ^* are enclosed in the red boxes. Each chain is shown in different colors. All the configurations of solutions consisting of monodisperse polymers with $N = 70$ are shown in the 2D box of the same size. As a result, only a part of the simulation is depicted except for the case with the highest ϕ . See Figures 3 and S1 for the configurations of polymer solutions with $N = 640$.

To sample polymer solution configurations, we integrated the underdamped Langevin equations:

$$m\ddot{\mathbf{r}}_i = -\zeta\dot{\mathbf{r}}_i - \nabla_{\mathbf{r}_i}\mathcal{H}(\mathbf{r}) + \boldsymbol{\xi}_i(t) \quad (5)$$

with the random force satisfying $\langle \boldsymbol{\xi}_i(t) \rangle = 0$ and $\langle \boldsymbol{\xi}_i(t) \cdot \boldsymbol{\xi}_j(t') \rangle = 4\zeta k_B T \delta_{ij} \delta(t - t')$. A small time step of $\delta t = 0.005\tau$ and a small friction coefficient of $\zeta = 0.1 m/\tau$ with the characteristic time scale $\tau = (ma^2/\epsilon)^{1/2}$ were employed to enhance the rate of equilibrium sampling of the polymer configurations.

The polymer solutions of long chains ($N = 80, 160, 320, 640, 1280$) were simulated in an NVT ensemble in two steps. (i) From the condition of a dilute solution ($\phi = \pi/400 \approx 7.85 \times 10^{-3}$) that contains 36 pre-equilibrated chains, the size of the periodic box was reduced step by step with $L \rightarrow \eta L$ ($\eta = 0.904$) so that the area fraction was increased by a factor of η^{-2} in each step. At each value of ϕ , excessive shrinking-induced overlaps between monomers were eliminated by gradually increasing the short-range repulsion part of \mathcal{H} . More specifically, the nonbonded potential $\mathcal{H}_{\text{nb}}(\mathbf{r})$ was replaced with $\min\{u_c, \mathcal{H}_{\text{nb}}(\mathbf{r})\}$, in which u_c was slowly elevated. (ii) For the

production run, the system was simulated for $500N\tau$, and chain configurations were collected every $0.1N\tau$. For each combination of N and ϕ , 10 replicas were generated from different initial configurations and random seeds.

To facilitate the sampling to calculate Π more accurately, polymer solutions of short chains ($N = 40, 50, 56, 70$) were simulated in an isothermal–isobaric (NPT) ensemble, in which the total number of monomers was fixed at 8400. During the production run for $1.5 \times 10^4 N\tau$, area-changing trial moves were generated every $N\tau$ time step via the Metropolis algorithm, which helped maintain the system at a constant pressure.²⁵ The structural properties averaged over all replicas were demonstrated in this study with the error bars denoting the standard deviations. The simulations were performed using the ESPResSo 3.3.1 package.²⁶

Standard Isothermal Compressibility κ_T . As simulations of short chain solutions were performed in an isothermal–isobaric (NPT) ensemble, we calculated the standard isothermal compressibility by

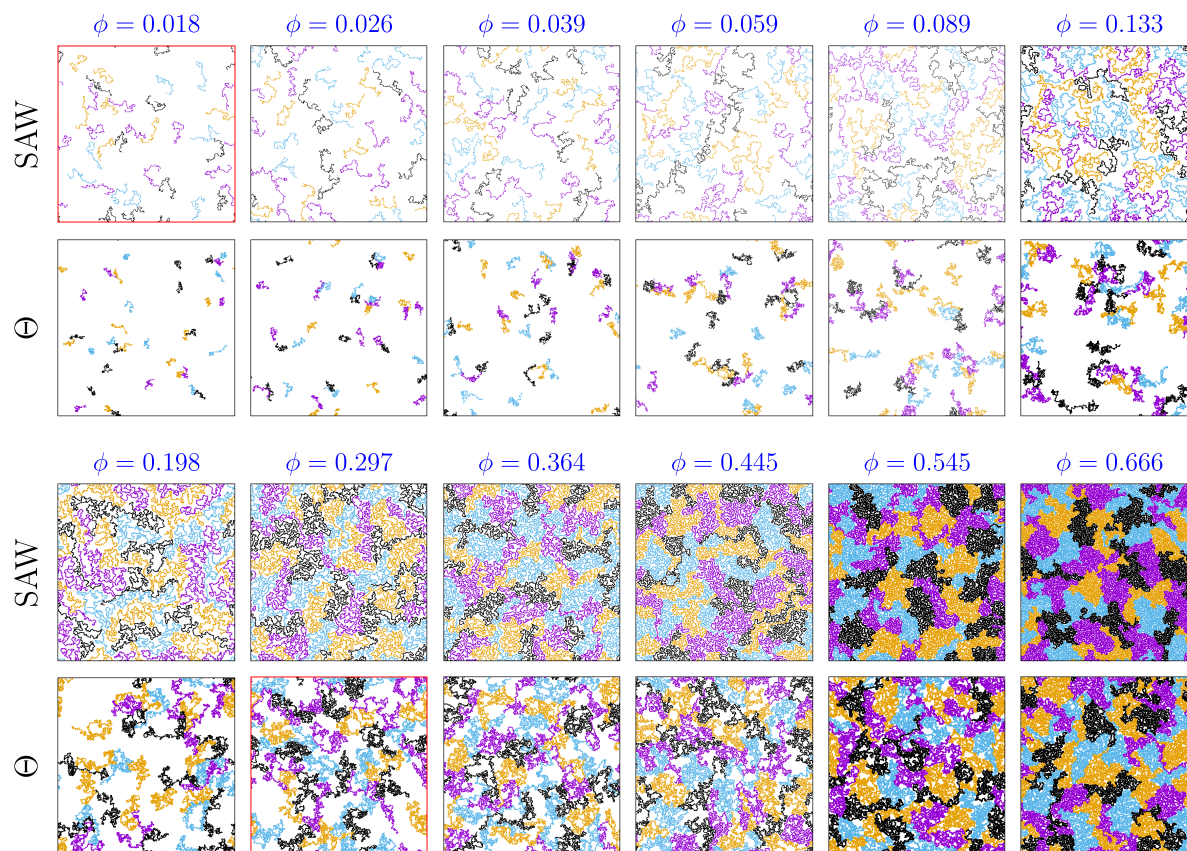


Figure 3. Polymer solutions of SAW and Θ chains in 2D with increasing area fraction ϕ (or equivalently the monomer density), from nonoverlapping ($\phi/\phi^* < 1$), semidilute ($\phi/\phi^* \approx 1$), and dense melt regimes ($\phi/\phi^* \gg 1$). Each chain with $N = 640$ is depicted in different colors. The threshold overlap area fractions for SAW and Θ solutions with $N = 640$ are estimated by extrapolating the relation $\phi_{\text{SAW}}^* \sim N^{-1/2}$ and $\phi_{\Theta}^* \sim N^{-1/7}$ and the knowledge of ϕ^* at $N = 70$ (Figure 2B) to $N = 640$, which yields $\phi_{\text{SAW}}^* \approx 0.018$ and $\phi_{\Theta}^* \approx 0.266$ for $N = 640$. Note that each panel is drawn by maintaining the relation of $\phi L^2 = \text{const}$. In other words, the number of polymers (monomers) in each panel is identical, and that a panel with smaller ϕ displays a larger simulation box size ($L \times L$). Figure S1 offers the snapshots of the simulations conducted at different ϕ 's in the 2D box at the identical field of view.

$$\kappa_T = \frac{1}{k_B T} \frac{\langle A^2 \rangle - \langle A \rangle^2}{\langle A \rangle} \quad (6)$$

where A is the fluctuating area of the simulated solution.²⁷

For longer chains, κ_T was calculated by $\kappa_T = \chi_T (\rho k_B T)^{-1}$, where the reduced isothermal compressibility χ_T was determined with a spatial block analysis method.²⁸ More specifically, whereas χ_T can be calculated by

$$\chi_T = \frac{\langle N^2 \rangle - \langle N \rangle^2}{\langle N \rangle} \quad (7)$$

where N is the particle number in a grand ensemble, various finite-size effects need to be considered to extrapolate χ_T in a simulated canonical (NVT) ensemble. χ_T^B calculated from subdomains in an NVT ensemble varies with the domain size B (Figure S3A). When the ratio of subdomain size $\lambda \equiv B/B_0$ approaches 1, where B_0 denotes the size of the full simulation box, χ_T approaches 0 as expected. Next, we extrapolated the values of χ_T^∞ by fitting the data to a function proposed in ref 28, $\chi_T^B = \chi_T^\infty \lambda(1 - \lambda^3) - c$ (Figure S3B). The final results are plotted as a function of the area fraction in Figure 4B.

RESULTS

Pressure Isotherm of a Polymer Solution Confined in Two Dimensions. Figure 2A demonstrates the osmotic pressure calculated for a 2D polymer solution consisting of monodisperse chains with varying ϕ and N ($N = 40, 50, 56$, and 70) under good and Θ solvent conditions, with the chain configurations with $N = 70$ shown in Figure 2C (see Figure 3 for the chain configurations with $N = 640$ for increasing ϕ). The polymer solutions were simulated on a 2D plane of area $A (= L^2)$ along with the periodic boundary condition. The osmotic pressure was computed by evaluating the virial equation:²⁴

$$\Pi = \rho k_B T - \frac{1}{2A} \sum_{i < j} r_{ij} \left. \frac{du(r)}{dr} \right|_{r=r_{ij}} \quad (8)$$

where $u(r)$ (see eq 1) is the interparticle potential between two monomers separated by a distance r .

While the scaling regime demonstrated in Figure 2A is not sufficiently clear because of the relatively short polymer chain lengths being simulated, the theoretically anticipated scaling behaviors for the polymer solution are semiquantitatively reproduced (see Appendix A). (i) For $\phi < \phi^*$ the osmotic pressure Π of the 2D polymer solution scales linearly with the area fraction ϕ as $\Pi \sim \phi/N$. Note that, for the same ϕ , Π is

indeed smaller for a larger chain length N (see Figure 2A). (ii) For $\phi^* < \phi \ll 1$, $\Pi_{\text{SAW}} \sim \phi^3$, $\Pi_{\Theta} \sim \phi^8$, and the Π – ϕ isotherm becomes independent of N (see Figure 2A and Appendix A). (iii) In all values of ϕ , we find that $\Pi_{\text{SAW}}(\phi) > \Pi_{\Theta}(\phi)$. (iv) The overlap area fraction ϕ^* decreases with N as $\phi^* \sim N^{1-2\nu}$. Using the scaling relations $\phi_{\Theta}^* \sim N^{-1/7}$ and $\phi_{\text{SAW}}^* \sim N^{-1/2}$, one can extrapolate ϕ^* for large N (see Figure 2B).

DISCUSSION

Radial Distribution of the Monomers Determines the Scaling Behavior of the Osmotic Pressure. The compressibility equation from the theory of liquids²⁷ associates the number fluctuations ($\langle(\delta N)^2\rangle$) with the isothermal compressibility (κ_T) and the radial distribution function ($g(r)$) as follows (see Appendix B for the details of the derivation):

$$\frac{\langle(\delta N)^2\rangle}{\langle N\rangle} = \rho k_B T \kappa_T = 1 + \rho \int (g(r) - 1) dr \quad (9)$$

From the definition of isothermal compressibility

$$\kappa_T = -\frac{1}{A} \left(\frac{\partial A}{\partial \Pi} \right)_{T,N} = \frac{1}{\phi} \left(\frac{\partial \phi}{\partial \Pi} \right)_{T,N} \quad (10)$$

where $\phi \simeq Na^2/A$, it is straightforward to show that the scaling relationship of $\Pi \sim \phi^q$ signifies $\kappa_T \sim \phi^{-q}$. The scaling regime demonstrated in the isothermal compressibility with the area fraction (Figure 4), which was calculated using longer chains, is, albeit not perfect, more clearly seen than that in Figure 2A.

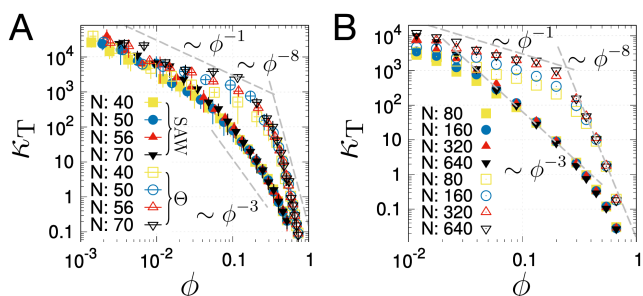


Figure 4. Standard isothermal compressibility κ_T vs the area fraction. (A) For short chains, simulations were performed in an isothermal–isobaric (NPT) ensemble. The compressibility was calculated by $\kappa_T = (\langle A^2 \rangle - \langle A \rangle^2) / \langle A \rangle k_B T$ where A is the fluctuating area of the simulated solution (ref 27). (B) For longer chains, κ_T was calculated from the particle number fluctuations in subdomains in a canonical ensemble by using a spatial block analysis method (ref 28). More details are explained in Figure S3 and its caption. Since the dimensionless reduced isothermal compressibility $\chi_T (= \rho k_B T \kappa_T)$, defined by the ratio between the bulk isothermal compressibility and that of the ideal gas $(\rho k_B T)^{-1}$, is expected to scale with the blob size $g(\rho)$,²⁴ κ_T scales as ϕ^{-3} and ϕ^{-8} in semidilute SAW and Θ chain solutions, respectively.

According to eq 9, the solvent quality dependent Π – ϕ isotherm originates from the difference in $g(r)$. Thus, there ought to be a difference between $g(r)$'s of SAW and the Θ polymer solutions, and the difference should yield the distinct exponent q . Nevertheless, it is not straightforward to see the difference between the $g(r)$'s of the two solvent conditions except for the amplitude (Figure 5A). Only when the $g(r)$ is decomposed into the contributions from the particles comprising the same chain ($g_{\text{intra}}(r)$) and a different chain

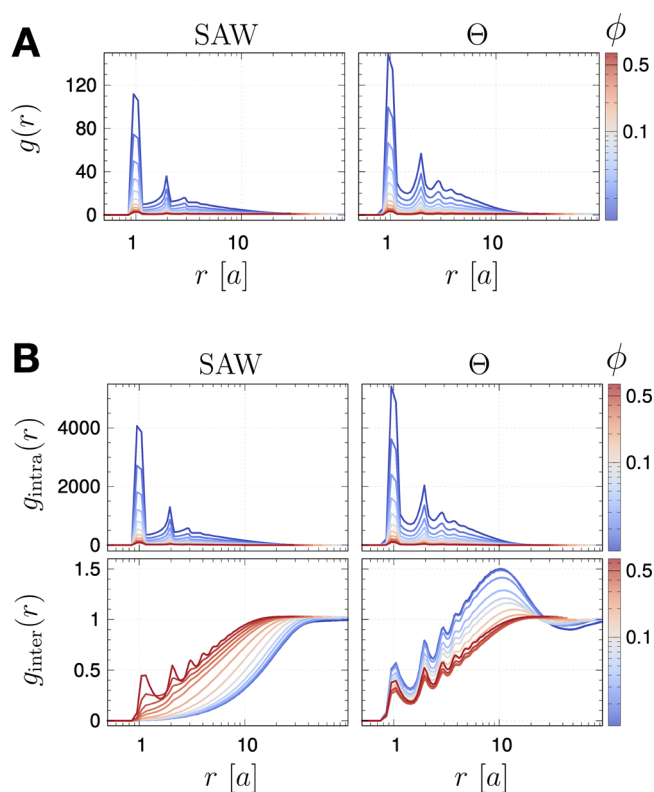


Figure 5. Radial distribution of monomers ($g(r)$) in SAW (left) and Θ polymer solutions (right) at varying ϕ . The distribution was calculated using polymer solutions with $N = 70$. (A) The full radial distribution of the monomers. (B) The full radial distribution of the monomers decomposed into the intra- (top) and interchain (bottom) radial distributions.

($g_{\text{inter}}(r)$) (Figure 5B) (or see their Fourier-transformed version of $g_{\text{intra}}(r)$, $F(k)$, calculated in Figure S2), does it become clear that there is a qualitative difference between $g_{\text{intra}}^{\text{SAW}}(r)$ and $g_{\text{inter}}^{\Theta}(r)$; however, such a decomposition is of limited use in that it is not directly accessible in experimental measurements.

Chain Conformations in Polymer Solutions. The conformations of polymer chains with increasing ϕ illustrated in Figure 2C draw a distinction between the two types of polymer solutions. Better visualization of the chain conformations in 2D polymer solutions calculated with longer polymer chains with $N = 640$ is given in Figures 3 and S2.

First, the individual chains in a Θ solvent are more crumpled than those in a good solvent. Over the intermediate regime of the wave vector k ($1/R_g < k < 1/\xi(\phi)$), corresponding to the length scale of $6a < r < 60a$, the structure factor $F(k)$ scales with k as $F(k) \sim k^{-4/3}$ and $F(k) \sim k^{-7/4}$ for polymer solutions under good and Θ solvent conditions, respectively (see Figure S2), reflecting the difference between the spatial arrangement of the monomers in the two polymer solutions.

In the semidilute phase ($\phi > \phi^*$), with increasing ϕ , the size of an individual chain (or domain size) decreases for the case of a SAW solution; however, such tendency is effectively absent in a Θ polymer solution for $0.02 \leq \phi \leq 0.44$ (see Figure 6A). The snapshots of individual chains from the simulations at varying ϕ shown in Figure 6A indicate that, compared to the chains in a Θ solvent, the extent of size reduction in the chain under a good solvent condition is greater. The size of the Θ chain is not sensitive to ϕ as if each chain barely feels the neighboring chains.

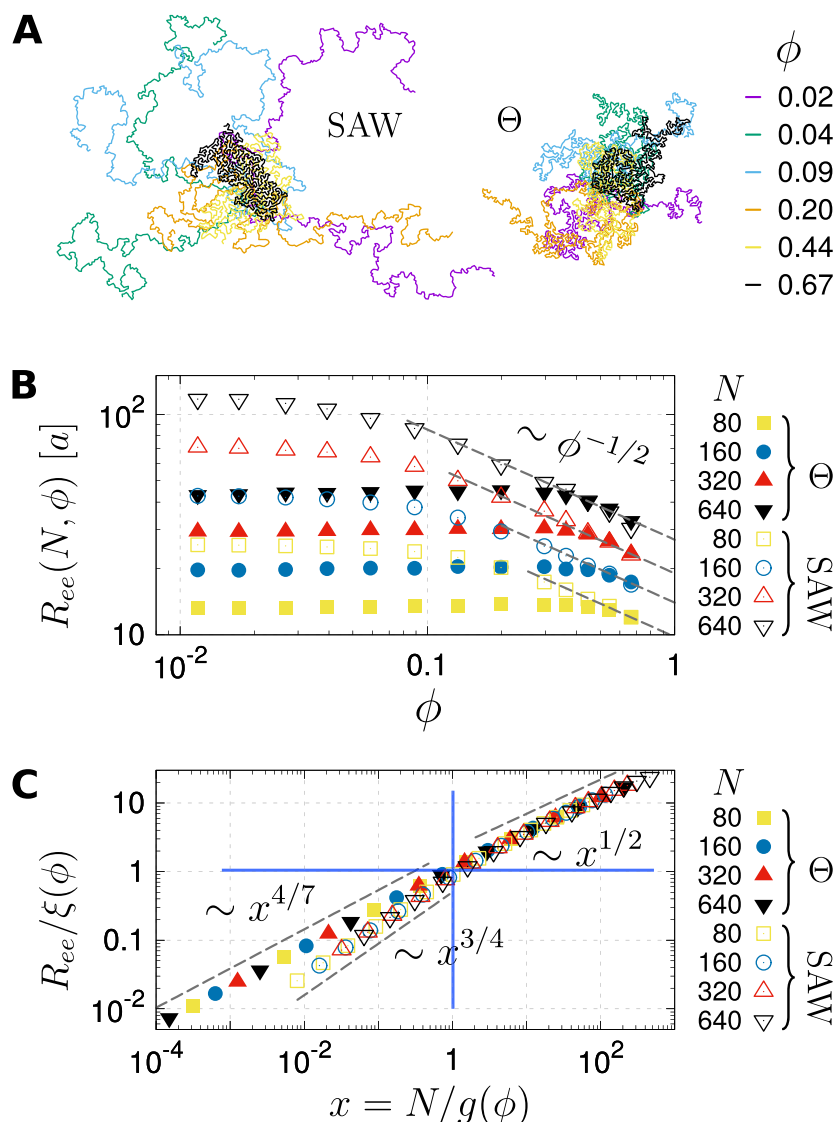


Figure 6. (A) Configurations of a polymer chain ($N = 640$) in a 2D polymer solution in good solvent and a Θ condition. The figure shows how the size of a single polymer changes with varying ϕ . At the same value of ϕ , polymer chains in a Θ condition are generally more compact than those in a good solvent condition. (B) The size of individual chain in terms of the end-to-end distance (R_{ee}) vs ϕ . At high ϕ , both polymers under good and Θ solvent conditions form dense polymer melts and their size scales with ϕ as $R_{ee} \sim \phi^{-1/2}$. (C) The chain size (end-to-end distance, R_{ee}) rescaled with a blob size ($\xi \simeq a\phi^{\nu/(1-2\nu)}$) plotted against N rescaled with the number of monomers in a blob ($g \simeq \phi^{1/(1-2\nu)}$) for varying densities collapses to the master curves for SAW and Θ solutions. In both cases, the crossover points to dense polymer melts are identified at $N/g(\phi) \simeq 1$ and $R_{ee}/\xi(\phi) \simeq 1$.

The insensitivity of Θ polymer size to the increasing ϕ can also be confirmed with the intrachain form factor ($F(k)$) calculated in Figure S2.

To be more quantitative, we calculate the mean end-to-end distance of individual chains as a function of ϕ (Figure 6B). Two points are noteworthy. (i) As long as the solution is not in the concentrated regime ($\phi \ll 1$), Θ chains in solution (filled symbols in Figure 6B) maintain their size. The minor expansions observed at $\phi < \phi^*$ are likely due to the effect of the neighboring chains that attract. (ii) At sufficiently high area fraction ($\phi \gg \phi^*$), the polymer solution becomes a melt, the data points with the same N from the two solvent conditions coincide, and the effect of solvent quality on polymer size is no longer observed. The sizes of chains are reduced as $R_{ee} \sim \phi^{-1/2}$.

Provided that a chain of length N in a 2D polymer solution is divided into N/g blobs of size ξ , each composed of g correlated

monomers ($\xi \simeq ag^\nu$), the area fraction of the monomers inside the blob is $\phi \simeq ga^2/\xi^2$. From these two relations, it follows that

$$\xi(\phi) \simeq a\phi^{\nu/(1-2\nu)} \quad (11)$$

and

$$g(\phi) \simeq \phi^{1/(1-2\nu)} \quad (12)$$

Since $\nu = 3/4$, $4/7 > 1/2$, the size and number of blobs decrease with ϕ . With this blob picture in mind, the ϕ -dependent size of the polymer $R_{ee}(\phi)$ is expected to scale as

$$R_{ee}(\phi) \simeq \xi(\phi)(N/g(\phi))^\nu \quad (13)$$

Plotted by rescaling $R_{ee}(\phi)$ with $\xi(\phi)$ and N with $g(\phi)$, the individual curves of $R_{ee}(N, \phi)$ obtained at varying N and ϕ in Figure 6B collapse on the two distinct master curves (Figure

6C). (i) For the value of ϕ in which the blob size is greater than that of a chain ($R_{ee}/\xi(\phi) < 1$, $N/g(\phi) < 1$), $R_{ee}/\xi(\phi) \simeq (N/g(\phi))^\nu$ with $\nu = 4/7$ for a Θ solvent and $\nu = 3/4$ for a good solvent condition (Figure 6C). (ii) For the opposite case ($R_{ee}/\xi(\phi) > 1$, $N/g(\phi) > 1$), all the data points obtained from different N 's and solvent qualities collapse onto the single master curve $R_{ee}/\xi(\phi) \simeq (N/g(\phi))^{1/2}$. From i and ii, it is suggested that the effect of solvent quality on the chain manifests itself only inside blobs, beyond which the individual polymers obey the statistics of polymer melts ($R_{ee} \sim N^{1/2}$).

In fact, the blob size $\xi(\phi)$ is equivalent to the correlation length of the polymer solution. In the semidilute phase, the correlation length $l(\phi)$ can be associated with the Flory radius as $l(\phi) \sim R_F(\phi^*/\phi)^{m_f}$.¹ Since $\phi^* \sim N^{1-2\nu}$, $R_F \simeq aN^\nu$, and $l(\phi)$ should be independent of the chain length (N) of an individual polymer in solution, one can determine m_f from $\nu + m_f(1-2\nu) = 0$. Thus, $l(\phi) \simeq a\phi^{\nu/(1-2\nu)}$, which is equivalent to eq 11, allowing us to interpret that the blob size $\xi(\phi)$ is tantamount to the correlation length of the polymer solution in the semidilute phase.

When $g^{1/2} \simeq \phi^{1/2}\xi/a$ is substituted to eq 13 with $\nu = 1/2$, it yields $R_{ee} \simeq aN^{1/2}\phi^{-1/2}$, which accounts for the $R_{ee} \sim \phi^{-1/2}$ ($\phi \gg \phi^*$) shown in Figure 6B.

Interstitial Voids. The varying sizes of interstitial voids interspersing the space between monomers in a Θ condition are another key feature that differentiates a Θ polymer solution from a SAW solution in 2D at the same ϕ (Figure 2C; see also Figures 3 and S2 calculated with $N = 640$ for clearer images). In comparison with the interstitial voids in a Θ chain solution, those in a SAW solution appear more uniform in size.

To make this observation more quantitative, we first identify the voids from the configurations of the polymer solution and calculate the void size distribution (Figure 7). The whole

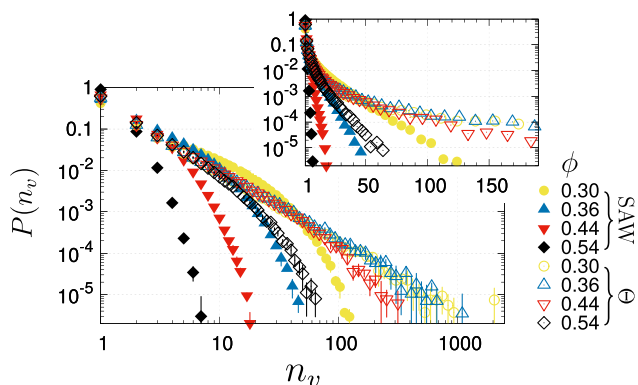


Figure 7. Probability distribution of void size (n_v) in semidilute polymer solutions ($\phi^* \leq \phi \ll 1$) with $N = 640$. The inset shows the log-linear plot. The corresponding configurations of the polymer solution are depicted in Figures 2 and S1.

simulation box was divided into the cells of a $1.5a \times 1.5a$ square lattice, and a void was defined as a cluster of empty cells that are connected without being intercepted by the polymer chains. The Hoshen–Kopelman algorithm, which is often utilized in studies of percolation,^{29,30} was employed to quantify the size of a void by means of the number of unoccupied cells (n_v). The void size distributions $P(n_v)$ in Figure 7 have exponentially decaying tails. The tail of $P(n_v)$ for the Θ chain solution at the same ϕ is an order of magnitude longer than that for the SAW solution.

Notably, the interstitial voids formed in a Θ chain solution display a more heterogeneous distribution with heavier tails, and hence, the average void size $\langle n_v \rangle (= \int n_v P(n_v) dn_v)$, which can be calculated from Figure 7, is greater than that of a SAW chain solution, i.e., $\langle n_v^\Theta \rangle(\phi) > \langle n_v^{\text{SAW}} \rangle(\phi)$ (Figure 8). Larger

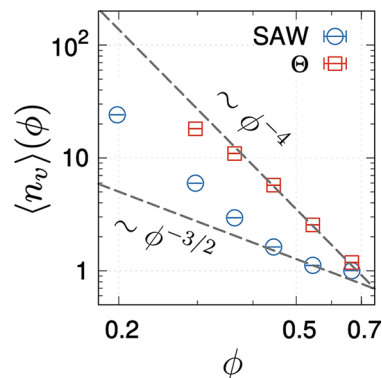


Figure 8. Average size of interstitial voids, $\langle n_v \rangle$, under good and Θ solvent conditions are calculated from $P(n_v)$ in Figure 7. As expected, the void size is a decreasing function of ϕ . For $\phi > \phi^*$ ($\phi_{\text{SAW}}^* \approx 0.02$, $\phi_\Theta^* \approx 0.27$ for $N = 640$) the void size scales with ϕ as $\langle n_v \rangle \sim \phi^{-4}$ and $\sim \phi^{-3/2}$ for Θ and SAW solutions, respectively.

interstitial voids in a polymer solution alleviate the intermolecular repulsion, lowering the osmotic pressure. From the analysis of our numerics, we find that the average size of the interstitial void scales approximately with ϕ as $\langle n_v \rangle \sim \phi^{-4}$ for a Θ chain solution and $\langle n_v \rangle \sim \phi^{-3/2}$ for a SAW solution for $\phi > \phi^*$ (Figure 8). Notably, the average size of the interstitial void displays the scaling relation identical to that of the blob size (or correlation length). In fact, the surface pressure in a semidilute phase is related with $\xi(\phi)$ as

$$\Pi \sim \frac{k_B T}{\xi(\phi)^2} \sim \frac{k_B T}{\phi^{2\nu/(1-2\nu)}} \quad (14)$$

Because of eq 14, the inequality of $\xi_\Theta(\phi) > \xi_{\text{SAW}}(\phi)$ (or $\langle n_v^\Theta \rangle(\phi) > \langle n_v^{\text{SAW}} \rangle(\phi)$) for $0 < \phi < 1$ implies the inequality of $\Pi_\Theta(\phi) < \Pi_{\text{SAW}}(\phi)$. For the case of a dilute solution ($\phi < \phi^*$), $\Pi \sim (\phi/N) + B_2(\phi/N)^2 + B_3(\phi/N)^3 + \dots$ (see Appendix A). Since $B_2 > 0$ and $B_3 > 0$ for a SAW chain and $B_2(\phi/N)^2 + B_3(\phi/N)^3 + \dots \approx 0$ for a Θ chain, the inequality $\Pi_\Theta(\phi) < \Pi_{\text{SAW}}(\phi)$ is expected as well.

CONCLUDING REMARKS

Our numerics, although the chains are still not long enough to generate scaling regimes clearly, have semiquantitatively reproduced the basic features characterizing the experimentally measured Π – ϕ isotherm of a thin polymer film.^{15,16} Polymer configurations of a 2D polymer solution visualized through our numerics clarify a qualitative difference between the polymer configurations in good and Θ solvents.

Among the two fundamental scaling exponents involved in polymer configurations, ν and γ , the one involved with the size ($R \sim N^\nu$) and the other with the entropy of the chain ($Z_N \sim \mu^N N^{\gamma-1}$),¹ ν is the only exponent that decides the dependence of the osmotic pressure on ϕ . It is worth noting that the exponent γ (more specifically γ_4 and γ_2 , where γ_L is the exponent for an L -star polymer³¹), which may be linked to the correlation hole

exponent θ and the fractal dimension of the external perimeter d_p ,^{1,31} however, makes no contribution to determining the osmotic pressure.

Visualizing the distributions of monomers (Figures 2, 3, and 5) and, more importantly, the distinct distributions of interstitial voids for two different polymer solutions (Figures 7 and 8), this study offers comprehensive understanding to the physical origin of the differing surface pressure isotherms of a 2D polymer solution under good and Θ solvent conditions.

APPENDIX

A: Osmotic Pressure of a Polymer Solution with Increasing ϕ

The osmotic pressure of a polymer solution displays substantial changes with increasing ϕ . Before our in-depth discussion on the solvent quality dependent osmotic pressure, we briefly review some basics of polymer solutions along with Figure A1.

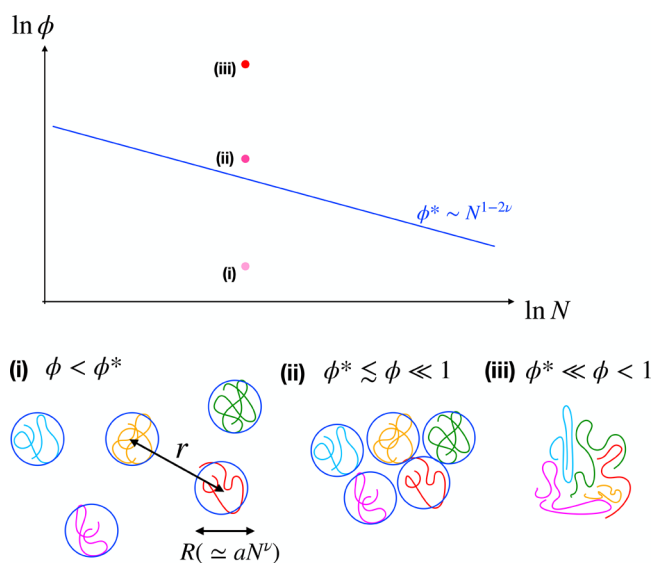


Figure A1. Diagram illustrating the polymer solution at three different regimes of area fraction. In isolation, the size of the polymer scales with N as $R \simeq aN^\nu$. The average distance between polymers is denoted by r . The threshold overlap area fraction (ϕ^* , blue line) scales with the length of the polymer chain as $\phi^* \sim N^{1-2\nu}$ in 2D ($d = 2$). Depending on the value of the area fraction ϕ , the polymer solution is classified into three regimes: (i) dilute ($\phi < \phi^*$), (ii) semidilute ($\phi^* < \phi \ll 1$), and (iii) concentrated ($\phi^* \ll \phi < 1$).

(i) In the nonoverlapping dilute regime ($\phi < \phi^*$) each chain is effectively isolated and the property of the polymer solution can be described with individual polymer chains that behave like a van der Waals gas of radius $R_F \sim N^\nu$ at a concentration of $\sim \phi/N$. In this regime, the osmotic pressure is given by $a^d \Pi/T \simeq \phi/N + B_2(\phi/N)^2 + O[(\phi/N)^3]$, where a is the monomer size and $B_2 \sim R_F^{d-1}$.

(ii) As ϕ increases, there is a point where the average distance between the chains and their size (R_F) becomes comparable, and the polymer solution reaches the overlap concentration ($\rho \approx \rho^*$ or $\phi \approx \phi^*$). Beyond this point, it becomes difficult to tell whether neighboring monomers belong to the same chain or to a different chain, and the global concentration of monomers becomes identical to the intrachain monomer concentration $\rho^* = N/R_F^d$. Hence, the corresponding volume fraction is

given as $\phi^* = \rho^* a^d = Na^d/R_F^d \sim N^{1-d\nu}$. For a polymer solution in the regime of the semidilute condition, $\phi^* < \phi \ll 1$, its osmotic pressure obeys the scaling law of $a^d \Pi/T \simeq (\phi/N)f(\phi/\phi^*)$. Π in this regime is impervious to the actual length of the polymer (N), and it is determined solely by the local volume (area) fraction ϕ .^{1,15,16} The scaling ansatz that the scaling function is given by $f(x) \sim x^m$ results in $(\phi/N)(\phi/\phi^*)^m \simeq \phi^{1+m}N^{-1+m(d\nu-1)} \sim N^0$, which determines $m = (d\nu - 1)^{-1}$ and yields the scaling relation $\Pi \sim \phi^{d\nu/(d\nu-1)}$.

(iii) When ϕ increases further, the pressure of the polymer solution starts to deviate from $\Pi \sim \phi^{d\nu/(d\nu-1)}$,³² and in the highly concentrated regime ($\phi \gg \phi^*$) the solution eventually forms a polymer melt. In 3D ($d = 3$), the interactions between monomers of polymer chains are effectively screened so that the chains behave like ideal polymers with the size of individual polymer chains scaling as $R_F (= \langle R_g^2 \rangle^{1/2}) \sim N^{1/2}$. The polymer chains *interpenetrate* each other, displaying a strong correlation with their neighbors.¹ By contrast, polymer melts in 2D are characterized by completely different physical properties because of the topological interaction overwhelming other interactions. Polymer chains *segregate* from each other and form compact, space-filling domains whose size scales as $R_F \sim N^{1/d}$ with $d = 2$. It is of particular note that, although the scaling exponents in the melts are identical to $\nu = 1/2$ for both 2D and 3D, the underlying physics giving rise to the exponent 1/2 are fundamentally different.²⁴ In 2D, the intrachain monomer distributions of a polymer chain in a polymer solution under both good and Θ solvent conditions differ from the distribution of a Gaussian polymer (Figure S4).³³

B. Connection between κ_T , $g(r)$, and Number Fluctuations

For N indistinguishable particles distributed in space, a grand partition function is written as

$$\Xi = \frac{1}{N!} \sum_{N=1}^{\infty} z^N \int d\mathbf{r}^N e^{-\beta V_N} \quad (\text{B1})$$

where $z \equiv e^{\beta\mu}$, $d\mathbf{r}^N \equiv \prod_{i=1}^N d\mathbf{r}_i$, $V_N \equiv V(\mathbf{r}_1, \mathbf{r}_2, \dots, \mathbf{r}_N)$, and the factor $N!$ is introduced to account for the indistinguishability of the particles. Then, the joint probability density of n indistinguishable particles in space is given by

$$\begin{aligned} \rho^{(n)}(\mathbf{r}_1, \mathbf{r}_2, \dots, \mathbf{r}_n) &= \frac{1}{\Xi} \left[\frac{1}{(N-n)!} \sum_{N>n} z^N \int d\mathbf{r}^{N-n} e^{-\beta V_N} \right] \\ &= \frac{N!}{(N-n)!} \frac{\sum_{N>n} z^N \int d\mathbf{r}^{N-n} e^{-\beta V_N}}{\sum_{N=1}^{\infty} z^N \int d\mathbf{r}^N e^{-\beta V_N}} \\ &\equiv P(\mathbf{r}_1, \mathbf{r}_2, \dots, \mathbf{r}_n) \end{aligned} \quad (\text{B2})$$

where $P(\mathbf{r}_1, \mathbf{r}_2, \dots, \mathbf{r}_n)$ is the joint probability density of n distinguishable particles. Then, it follows from eq B2 that

$$\int d\mathbf{r}^n \rho^{(n)}(\mathbf{r}_1, \mathbf{r}_2, \dots, \mathbf{r}_n) = \left\langle \frac{N!}{(N-n)!} \right\rangle \quad (\text{B3})$$

Now, we consider the joint probability density of two indistinguishable particles at \mathbf{r}_1 and \mathbf{r}_2 with an assumption that their distribution in space is *homogeneous* and *isotropic*, satisfying $\rho^{(2)}(\mathbf{r}_1, \mathbf{r}_2) \approx \rho^2 g(r_{12})$, where $\rho \equiv N/V$, $r_{12} \equiv |\mathbf{r}_1 - \mathbf{r}_2|$ and $g(r)$ is the radial distribution function. Then, together with the

probability density for a single particle in homogeneous and isotropic space, satisfying $\rho(\mathbf{r}) = \rho = N/V$ for $d = 3$ (or $\rho = N/A$ for $d = 2$), we obtain

$$\begin{aligned} \iint [\rho^{(2)}(\mathbf{r}_1, \mathbf{r}_2) - \rho^{(1)}(\mathbf{r}_1)\rho^{(1)}(\mathbf{r}_2)] d\mathbf{r}_1 d\mathbf{r}_2 &= \langle N \rangle \rho \int d\mathbf{r} [g(\mathbf{r}) - 1] \\ &= \langle N^2 \rangle - \langle N \rangle - \langle N \rangle^2 \end{aligned} \quad (\text{B4})$$

which yields $\langle (\delta N)^2 \rangle / \langle N \rangle = 1 + \rho \int [g(\mathbf{r}) - 1] d\mathbf{r}$ (eq 9).

Next, the total differential $d\Xi = -S dT + A d\Pi - N d\mu$ of the grand ensemble $\Xi = \Xi(T, \Pi, \mu)$ gives the following relations at constant temperature:

$$\begin{aligned} N \left(\frac{\partial \beta \mu}{\partial N} \right)_{T,A} &= \beta A \left(\frac{\partial \Pi}{\partial N} \right)_{T,A} \\ &= -\beta A \left(\frac{\partial \Pi}{\partial A} \right)_{T,N} \left(\frac{\partial A}{\partial N} \right)_{T,\Pi} \\ &= \frac{1}{\rho k_B T \kappa_T} \end{aligned} \quad (\text{B5})$$

with $\rho \equiv N/A$. Together with $(\partial \log \Xi / \partial \beta \mu)_{T,A} = \langle N \rangle$ and $(\partial \langle N \rangle / \partial \beta \mu)_{T,A} = \langle (\delta N)^2 \rangle$, it follows from eq B5 that

$$\frac{\langle (\delta N)^2 \rangle}{\langle N \rangle} = \rho k_B T \kappa_T \quad (\text{B6})$$

■ ASSOCIATED CONTENT

SI Supporting Information

The Supporting Information is available free of charge at <https://pubs.acs.org/doi/10.1021/acs.jpbc.2c05472>.

Scattering functions to probe the intrachain configurations of a polymer and additional figures of numerical results and analyses, including the configurations of polymer solutions, intrachain form factors, isothermal compressibility χ_T for increasing ϕ , and intrachain monomer distributions (PDF)

■ AUTHOR INFORMATION

Corresponding Authors

Lei Liu – Key Laboratory of Optical Field Manipulation of Zhejiang Province, Department of Physics, Zhejiang Sci-Tech University, Hangzhou 310018, China; Email: leiliu@zstu.edu.cn

Changbong Hyeon – School of Computational Sciences, Korea Institute for Advanced Study, Seoul 02455, Republic of Korea; orcid.org/0000-0002-4844-7237; Email: hyeoncb@kias.re.kr

Complete contact information is available at: <https://pubs.acs.org/10.1021/acs.jpbc.2c05472>

Notes

The authors declare no competing financial interest.

■ ACKNOWLEDGMENTS

We thank Professor Bae-Yeun Ha for a number of useful comments. This work is in part supported by the National Natural Science Foundation of China, ZSTU Intramural Grant (12104404, 20062226-Y to L.L.), and a KIAS Individual Grant (CG035003 to C.H.) at the Korea Institute for Advanced Study.

We thank the Center for Advanced Computation in KIAS for providing computing resources.

■ REFERENCES

- (1) de Gennes, P. G. *Scaling Concepts in Polymer Physics*; Cornell University Press: Ithaca and London, 1979.
- (2) Duplantier, B. Geometry of polymer chains near the theta-point and dimensional regularization. *J. Chem. Phys.* **1987**, *86*, 4233–4244.
- (3) de Gennes, P. G. Collapse of a polymer chain in poor solvents. *J. Phys., Lett.* **1975**, *36*, 55–57.
- (4) Douglas, J. F.; Cherayil, B. J.; Freed, K. F. Polymers in two dimensions: renormalization group study using three-parameter model. *Macromolecules* **1985**, *18*, 2455–2463.
- (5) Liu, L.; Pincus, P. A.; Hyeon, C. Compressing Θ -chain in slit geometry. *Nano Lett.* **2019**, *19*, 5667–5673.
- (6) Jung, Y.; Hyeon, C.; Ha, B.-Y. Near- Θ Polymers in a Cylindrical Space. *Macromolecules* **2020**, *53*, 2412–2419.
- (7) Coniglio, A.; Jan, N.; Majid, I.; Stanley, H. E. Conformation of a polymer chain at the θ' point: Connection to the external perimeter of a percolation cluster. *Phys. Rev. B* **1987**, *35*, 3617.
- (8) Sapoval, B.; Rosso, M.; Gouyet, F. The fractal nature of a diffusion front and the relation to percolation. *J. Phys., Lett.* **1985**, *46*, 149–156.
- (9) Bunde, A.; Gouyet, J. F. On scaling relations in growth models for percolating clusters and diffusion fronts. *J. Phys. A: Math. Gen.* **1985**, *18*, L285–L287.
- (10) Duplantier, B.; Saleur, H. Exact Tricritical Exponents for Polymers at the Θ Point in Two Dimensions. *Phys. Rev. Lett.* **1987**, *59*, 539–542.
- (11) Saleur, H.; Duplantier, B. Exact determination of the percolation hull exponent in two dimensions. *Phys. Rev. Lett.* **1987**, *58*, 2325.
- (12) Duplantier, B.; Saleur, H. Stability of the polymer Θ point in two dimensions. *Phys. Rev. Lett.* **1989**, *62*, 1368.
- (13) Duplantier, B. Two-dimensional fractal geometry, critical phenomena and conformal invariance. *Phys. Rep.* **1989**, *184*, 229–257.
- (14) Beffara, V. Hausdorff dimensions for SLE₆. *Ann. Probab.* **2004**, *32*, 2606–2629.
- (15) Vilanove, R.; Rondelez, F. Scaling description of two-dimensional chain conformations in polymer monolayers. *Phys. Rev. Lett.* **1980**, *45*, 1502.
- (16) Witte, K. N.; Kewalramani, S.; Kuzmenko, I.; Sun, W.; Fukuto, M.; Won, Y.-Y. Formation and collapse of single-monomer-thick monolayers of poly (n-butyl acrylate) at the air-water interface. *Macromolecules* **2010**, *43*, 2990–3003.
- (17) Cicuta, P.; Hopkinson, I. Scaling of dynamics in 2d semi-dilute polymer solutions. *EPL (Europhysics Letters)* **2004**, *68*, 65.
- (18) Carmesin, I.; Kremer, K. Static and dynamic properties of two-dimensional polymer melts. *J. Phys. (Paris)* **1990**, *51*, 915–932.
- (19) Nelson, P. H.; Hatton, T. A.; Rutledge, G. C. General reptation and scaling of 2d athermal polymers on close-packed lattices. *J. Chem. Phys.* **1997**, *107*, 1269–1278.
- (20) Wang, Y.; Teraoka, I. Structures and thermodynamics of nondilute polymer solutions confined between parallel plates. *Macromolecules* **2000**, *33*, 3478–3484.
- (21) Yethiraj, A. Computer simulation study of two-dimensional polymer solutions. *Macromolecules* **2003**, *36*, 5854–5862.
- (22) Semenov, A.; Johner, A. Theoretical notes on dense polymers in two dimensions. *Eur. Phys. J. E* **2003**, *12*, 469–480.
- (23) Sung, B. J.; Yethiraj, A. Structure of void space in polymer solutions. *Phys. Rev. E* **2010**, *81*, 031801.
- (24) Schulmann, N.; Meyer, H.; Kreer, T.; Cavallo, A.; Johner, A.; Baschnagel, J.; Wittmer, J. Strictly two-dimensional self-avoiding walks: Density crossover scaling. *Polymer Science Series C* **2013**, *55*, 181–211.
- (25) Frenkel, D.; Smit, B. *Understanding Molecular Simulation: From Algorithms to Applications*; Academic Press, Elsevier: San Diego, CA, 2002; Vol. 1.
- (26) Limbach, H.-J.; Arnold, A.; Mann, B. A.; Holm, C. ESPResSo—an extensible simulation package for research on soft matter systems. *Comput. Phys. Commun.* **2006**, *174*, 704–727.

(27) Hansen, J.-P.; McDonald, I. R. *Theory of Simple Liquids*; Academic Press, Elsevier: San Diego, CA, 1990.

(28) Heidari, M.; Kremer, K.; Potestio, R.; Cortes-Huerto, R. Fluctuations, finite-size effects and the thermodynamic limit in computer simulations: Revisiting the spatial block analysis method. *Entropy* **2018**, *20*, 222.

(29) Hoshen, J.; Kopelman, R. Percolation and cluster distribution. I. Cluster multiple labeling technique and critical concentration algorithm. *Phys. Rev. B* **1976**, *14*, 3438.

(30) Binder, K.; Heermann, D. *Monte Carlo Simulation in Statistical Physics*; Springer-Verlag: Berlin Heidelberg, Germany, 2010.

(31) Duplantier, B. Statistical Mechanics of Polymer Networks of Any Topology. *J. Stat. Phys.* **1989**, *54*, 581–679.

(32) Paturej, J.; Sommer, J.-U.; Kreer, T. Universal Equation of State for Flexible Polymers Beyond the Semidilute Regime. *Phys. Rev. Lett.* **2019**, *122*, 087801.

(33) Beckrich, P.; Johner, A.; Semenov, A. N.; Obukhov, S. P.; Benoit, H.; Wittmer, J. Intramolecular form factor in dense polymer systems: Systematic deviations from the Debye formula. *Macromolecules* **2007**, *40*, 3805–3814.

Recommended by ACS

Water Dissolved in a Variety of Polymers Studied by Molecular Dynamics Simulation and a Theory of Solutions

Hidekazu Kojima, Nobuyuki Matubayasi, *et al.*

AUGUST 05, 2021
THE JOURNAL OF PHYSICAL CHEMISTRY B

READ 

Predicting the Mobility Increase of Coarse-Grained Polymer Models from Excess Entropy Differences

Gustavo G. Rondina, Florian Müller-Plathe, *et al.*

FEBRUARY 07, 2020
JOURNAL OF CHEMICAL THEORY AND COMPUTATION

READ 

Co-nonsolvency Transition in Polymer Solutions: A Simulation Study

Zahra Mohammadyarloo and Jens-Uwe Sommer

OCTOBER 13, 2022
MACROMOLECULES

READ 

Polymer Fractionation at an Interface in Simple Shear with Slip

Shadrach Kwakye-Nimo, Paula M. Wood-Adams, *et al.*

JULY 25, 2022
MACROMOLECULES

READ 

Get More Suggestions >